HHS Public Access

Author manuscript

Magn Reson Med. Author manuscript; available in PMC 2018 September 01.

Published in final edited form as:

Magn Reson Med. 2017 September ; 78(3): 871–880. doi:10.1002/mrm.26799.

Improving the Detection Sensitivity of pH-weighted Amide Proton Transfer MRI in Acute Stroke Patients using Extrapolated Semisolid Magnetization Transfer Reference Signals

Hye-Young Heo[1,2], **Yi Zhang**[1], **Tina M. Burton**[3], **Shanshan Jiang**[1], **Yansong Zhao**[4], **Peter C.M. van Zijl**[1,2], **Richard Leigh**[3], and **Jinyuan Zhou**[1,2]

[1]Division of MR Research, Department of Radiology, Johns Hopkins University, Baltimore, Maryland, USA

[2]F.M. Kirby Research Center for Functional Brain Imaging, Kennedy Krieger Institute, Baltimore, Maryland, USA

[3]Neuro Vascular Brain Imaging Unit, National Institute of Neurological Disorders and Stroke, National Institutes of Health, Bethesda, Maryland, USA

[4]Philips Healthcare, Cleveland, Ohio, USA

Abstract

Purpose—To quantify APT effects in acidic ischemic lesions and assess the spatial-temporal relationship between diffusion, perfusion, and pH deficits in acute stroke patients.

Methods—Thirty acute stroke patients were scanned at 3 T. Quantitative APT ($APT^{\#}$) effects in acidic ischemic lesions were measured using an extrapolated semisolid magnetization transfer reference signal (EMR) technique and compared with commonly used MTR_{asym}(3.5ppm) or APT-weighted parameters.

Results—$APT^{\#}$ images showed clear pH deficits in the ischemic lesion, whereas MTR_{asym}(3.5ppm) signals were slightly hypointense. The $APT^{\#}$ contrast between acidic ischemic lesions and normal tissue in acute stroke patients was more than 3 times larger than MTR_{asym}(3.5ppm) contrast (−1.45 ± 0.40 % for $APT^{\#}$ vs. −0.39 ± 0.52 % for MTR_{asym}(3.5ppm), $p < 4.6 \times 10\text{-}4$). Hypoperfused and acidic areas without an apparent diffusion coefficient abnormality were observed and assigned to an ischemic acidosis penumbra. Hypoperfused areas at normal pH were also observed and assigned to benign oligemia. Hyperintense APT signals were observed in a hemorrhage area in one case.

Conclusion—The quantitative APT study using the EMR approach enhances APT MRI sensitivity to pH compared to conventional APT-weighted MRI, allowing more reliable delineation of an ischemic acidosis in the penumbra.

Corresponding and Reprint Author: Jinyuan Zhou, Ph.D., Division of MR Research, Department of Radiology, Johns Hopkins University School of Medicine, 600 N. Wolfe Street, Park 336, Baltimore, MD 21287, USA. Phone: (+1-410) 955-7491, Fax: (+1-410) 614-1977, jzhou@mri.jhu.edu.

SUPPORTING INFORMATION

Additional Supporting Information may be found in the online version of this article.

Keywords

APT; CEST; ischemic penumbra; pH; stroke

INTRODUCTION

The goal of acute ischemic stroke therapy is to salvage tissue that is at risk of infarction but still viable with reperfusion strategies. Such tissue is commonly referred to as the ischemic penumbra and has been the primary target of therapeutic interventions (1–5). In the absence of multimodal imaging, thrombolytic therapy with tissue plasminogen activator (tPA) is beneficial only when the treatment is initiated within the 3- and 4.5-hrs time window after symptom onset (6, 7).Using a time-based approach results in only a limited number of stroke patients being eligible for thrombolytic treatment (8). Patients presenting beyond these standard treatment time windows can benefit from therapy when selected using multimodal MRI (9), however precise identification of the ischemic penumbra is essential since the potential beneficial effect of treatment must be weighed against the risk of brain hemorrhage (8, 10). Consequently, early and accurate delineation of the at-risk, yet salvageable ischemic penumbra from the irreversibly damaged infarct core, can enhance patient selection for stroke treatments and extend the time window for therapeutic intervention.

Typically, diffusion-weighted imaging (DWI) allows visualization of early tissue damage by changing the local diffusion of water in the ischemic lesion while perfusion-weighted imaging (PWI) provides quantitative information on abnormal cerebral blood flow or volume. The DWI/PWI spatial mismatch has been used as a guide to identify the presence of salvageable tissues and to serve as a selection marker for thrombolysis (2, 11–13). However, the use of the DWI/PWI mismatch concept has proven to be limited in routine clinical application due to variable sensitivity, specificity and high false-negative rates (14–17). Specifically, the mismatch area is too large due to inclusion of regions of benign oligemia, and most basic literature indicates that a more appropriate penumbra would be that in which oxidative metabolism is impaired, but no diffusion changes have occurred (18–21). Thus, there is a need for imaging techniques that more accurately identify the ischemic penumbra from benign oligemia in order to advance the treatment of acute stroke by expanding the population of treatable patients.

The original concept of the ischemic penumbra was based on the concept of functionally impaired tissue, due to a deficit in oxidative metabolism, which is potentially viable but surrounds, and is contiguous with, an area of irreversible cerebral infarction (1, 22). Acute cerebral ischemia causes a shift to anaerobic glycolysis resulting in the accumulation of lactic acid and a concomitant decrease in intracellular pH (23). Therefore, tissue acidosis is the earliest sign that tissue is at risk but potentially salvageable when it can be contrasted with regions identified as being irreversibly infarcted. Recently, pH-sensitive amide proton transfer-weighted (APTw) imaging has shown promise in detecting ischemic tissue acidosis following impaired aerobic metabolism in animal models (24–29) and human stroke patients (30–33). Most of the previous APTw studies used the so-called magnetization transfer ratio asymmetry at 3.5 ppm or MTR_{asym}(3.5ppm). However, it is known that MTR_{asym}(3.5ppm)

is unavoidably contaminated by the upfield nuclear Overhauser enhancement (NOE) signals of mobile to semisolid macromolecules (34, 35), resulting in a small or sometimes negligible imaging signal. In this study, quantitative APT ($APT^{\#}$) and NOE (NOE#) effects in acidic ischemic lesions were investigated in acute stroke patients at 3 T, using the so-called extrapolated semisolid magnetization transfer reference (EMR) data analysis (36, 37). In this approach, semisolid magnetization transfer contrast (MTC) and direct water saturation contributions were fitted and extrapolated to obtain reference (baseline) signals at the APT and NOE frequencies, from which the CEST-based $APT^{\#}$ and NOE# signals could be derived by subtraction from the experimental signals. The results were compared with the commonly used $MTR_{asym}(3.5ppm)$ parameters. In addition, the spatial relationship between DWI, PWI, and pH deficits in these acute stroke patients were assessed.

METHODS

Conventional MTC model and EMR approach

The MTC model in tissue has been theoretically established using a two-pool exchange model based on the coupled Bloch equations including magnetization exchange between a free bulk water proton pool (w) and a semi-solid macromolecular proton pool (m) and RF absorption rate terms (38, 39). By assuming a steady-state condition, the longitudinal magnetization of the free bulk water protons (M_z^w), which has the equilibrium magnetization (M_0^w), can be written as follows:

$$\frac{M_z^w}{M_0^w}=\frac{\frac{1}{T_{1m}}\left(RM_0^mT_{1w}\right)+R_{rfm}+\frac{1}{T_{1m}}+R}{\left(RM_0^mT_{1w}\right)\left(R_{rfm}+\frac{1}{T_{1m}}\right)+\left[1+\left(\frac{\omega_1}{2\pi\Delta w}\right)^2\left(\frac{T_{1w}}{T_{2w}}\right)\right]\left(R_{rfm}+\frac{1}{T_{1m}}+R\right)} \quad [1]$$

where T_{1w} and T_{2w} are the longitudinal and transverse relaxation times of the free water proton pool, respectively; T_{1m} and T_{2m} are the longitudinal and transverse relaxation times of the semi-solid macromolecular proton pool, respectively; and M_0m is the fully-relaxed equilibrium magnetization value associated with the semi-solid macromolecular pool; R is the rate constant describing the magnetization exchange between the two proton pools (RM_0m for the exchange from the water pool to macromolecule pool and RM_0w for the reverse direction); and the RF absorption rate (R_{rfm}) is the loss rate of the longitudinal magnetization due to RF irradiation, which depends on the off-resonance RF irradiation of amplitude (w_1) and frequency offset ($\Delta\omega$), and on the transverse relaxation time of the semisolid macromolecular pool. The RF absorption rate is closely modeled by a super-Lorentzian lineshape, $g_m(2\pi\Delta\omega)$, for the semi-solid macromolecular protons:

$$R_{rfm}=\omega_1^2\pi g_m(2\pi\Delta\omega) \quad [2]$$

$$g_m\left(2\pi\Delta\omega\right)=\int_0^{\pi/2}d\theta sin\theta\sqrt{\frac{2}{\pi}}\frac{T_{2m}}{\left(3cos^2\theta-1\right)}e^{-2\left(\frac{2\pi\Delta\omega T_{2m}}{3cos^2\theta-1}\right)^2} \quad [3]$$

where θ is the dipole orientation angle between the magnetic moment and the external magnetic field. The MTC signal expression can be uniquely determined in terms of five combined model parameters, R, $RM_0^mT_{1w}$, T_{1w}/T_{2w}, T_{1m}, and T_{2m}.

After the five MTC model parameters are obtained by fitting the observed wide-offset MTC data, the EMR spectra (Z_{EMR}) can be calculated with the corresponding RF saturation power and frequency offset (36, 37). Quantitative chemical exchange saturation transfer (CEST#) signals can be described by subtracting the B_0-corrected experimental Z-spectra (namely, Z_{exp}) from the extrapolated two-pool MTC spectra (namely, Z_{EMR}), where $Z = S_{sat}/S_0$ and S_{sat} are the image signal intensities measured with RF saturation:

$$CEST^{\#}=Z_{EMR}(\Delta\omega) - Z_{exp}(\Delta\omega) \quad [4]$$

The commonly used APTw parameter (namely, MTR_{asym} at 3.5 ppm (24)), and newly introduced $APT^{\#}$ and NOE# parameters (36, 37) can be described by:

$$MTR_{asym}(3.5\ ppm)=Z_{exp}(-3.5\ ppm) - Z_{exp}(+3.5\ ppm) \quad [5]$$

$$APT^{\#}=Z_{EMR}(+3.5\ ppm) - Z_{exp}(+3.5\ ppm) \quad [6]$$

$$NOE^{\#}=Z_{EMR}(-3.5\ ppm) - Z_{exp}(-3.5\ ppm) \quad [7]$$

Note that $Z_{EMR}(+\Delta\omega)$ and $Z_{EMR}(-\Delta\omega)$ are identical when the symmetric MTC model is used. As described in our two previous papers (36, 37), when the symmetric MTC model is used, the large symmetrical semi-solid MTC is removed, and all others remain. Thus, when using the EMR method, a relatively clean $APT^{\#}$ signal can be quantified while the NOE# signal includes both the local NOE (from mobile molecules) and the conventional MTR asymmetry (from relatively less mobile protons).

Subjects

Subjects were recruited for this study by the NIH stroke team at MedStar Washington Hospital Center from January of 2015 through April of 2016. Thirty patients with acute ischemic stroke (<7 hours from symptom onset) were recruited into the NIH Natural History of Stroke Study following informed consent in accordance with IRB requirement and subsequently underwent APTw imaging. For each patient, serial MRI scans were variably performed at presentation, ~2 hours, ~24 hours, ~5 days, and ~1 month to characterize tissue evolution and progression to infarction. The initial MRI scan performed on presentation consisted of clinical sequences only that did not include APTw imaging to ensure timely administration of acute stroke treatments.

MRI Experiments

All acute stroke patients were scanned on a Philips 3 Tesla MRI scanner (Achieva 3.0T; Philips Healthcare, Best, The Netherlands) using a body coil for RF transmission and a 16-channel phased array coil for reception (Invivo, Gainesville, FL). The acute stroke imaging protocol included the following sequences: a T_2-weighted fluid-attenuated inversion recovery (FLAIR) sequence, a gradient recalled echo (GRE) hemosiderin weighted sequence, a time-of-flight MR angiography sequence, a diffusion tensor imaging sequence used to generate trace diffusion weighted images (DWI) using three orthogonal directions (b = 0 and 1000 s/mm2), and a T_2*-weighted dynamic susceptibility-contrast imaging sequence using a bolus of Gadobutrol (Gd-DO3A-butrol; 0.1mmol/kg), injected at 5 mL/s, followed by 15 mL saline. The ADC, time to peak (TTP), and maps of relative bolus transit time (rBTT) with respect to contralateral normal tissue were automatically generated by inline processing on the scanner console. Saturation MRI scans were performed prior to gadolinium injection using a fat-suppressed, turbo spin-echo pulse sequence with the following parameters: TR = 3 s; TE = 6.4 ms; FOV = 212 × 190 mm2; matrix size = 256 × 256; slice thickness = 4.4 mm; turbo-spin-echo factor = 45; and single-slice acquisition. The off-resonance RF saturation consisted of four block RF saturation pulses with duration of 200 ms (namely, RF saturation time or T_{sat} = 800 ms) and amplitude of 2 μT. Crusher gradients (10 ms duration and 10 mT/m strength) were applied between pulses to suppress the residual transverse magnetization. The frequency sweep for saturation corresponded to a wide range of frequency offsets from 14 ppm to −8 ppm with an interval of 0.5 ppm, and an unsaturated image was acquired for signal normalization. This was used to calculate the spectrum of saturated water intensity relative to non-saturated water intensity (Z-spectrum). To obtain sufficient signal-to-noise ratios for the APT and NOE images, four acquisitions were placed at +3.5 ppm and −3.5ppm, respectively. Additionally, another series of saturated images were acquired using a brief low RF saturation power (26 offsets from 1.2 to −1.2 ppm at intervals of 0.125 ppm, one average, B_1 = 0.5 μT) to determine B_0 maps using the water saturation shift referencing (WASSR) approach (40). 52 CEST images (scan time = 2 min 39 sec) and 26 WASSR images (scan time = 35 sec) were acquired, resulting in a total scan time of 3 min 14 sec. APTw imaging was collected as a single slice through the stroke guided by the DWI.

APT Data Processing

All saturation images were realigned to the saturated image at 3.5 ppm with the rigid body registration algorithm based on a mutual information cost function (41) using MATLAB (The MathWorks, Inc., Natick, MA) and co-registered with DWI and PWI images using Analysis of Functional Neuroimages (AFNI).Then, CEST saturated images were normalized voxel-by-voxel by the corresponding unsaturated (S_0) image and corrected for B_0 field inhomogeneities using the WASSR method (40). Next, two-pool MTC spectra (free bulk water and semisolid) were generated by the EMR technique (36, 37, 42–44). The semi-solid MTC model fitting under a non-steady-state (NS) condition can be described from the modified Bloch equations (45, 46). Our previous study (Supporting Information in (36)) compared semi-solid MTC model parameters fitted with the steady-state (SS) and NS equations for normal white matter data acquired with NS experimental parameters (B_1 = 2 μT; T_{sat} = 800 ms). While the results showed that a small difference existed, the simple SS

equation (Eq. [1]) can closely estimate the semi-solid MTC model parameters for the EMR signals. Wide-offset experimental Z-spectra with semisolid MTC data points between 8 and 14 ppm were chosen to avoid possible downfield CEST and upfield NOE signal contributions, and a data point at an offset of 0.5 ppm was chosen to improve the EMR fitting quality. These data points were fitted to a two-pool exchange model with a symmetric super-Lorentzian lineshape using the Levenberg-Marquardt algorithm as the sum of squares of nonlinear functions. The quality of the estimated MTC model was evaluated by the root of the sum of the squared differences between the fitted model and the experimental data, and goodness-of-fit metric. Note that the M_w0 was normalized to 1 and T_1 of semisolid MTC was fixed to 1.4 s because it is not well determined in fits to the MTC model (47).

Data Analysis and Statistical Analysis

Two regions of interest (ROIs), a contralateral normal tissue and an ischemic lesion that was DWI hyperintense, compared to the contralateral brain, were carefully drawn on the co-registered S_0 image, and the MTR_{asym}(3.5ppm), $APT^{\#}$, and NOE# signal intensities were reported. The $APT^{\#}$, NOE#, and MTR_{asym}(3.5ppm) were statistically compared using a one-way analysis of variance (ANOVA), followed by Tukey's post-hoc test. Statistical analyses were performed using the Statistical Package for the Social Sciences (SPSS, Chicago, IL). Statistical significance was accepted for $p < 0.01$.

For pixel-by-pixel analysis, pH/diffusion and perfusion/pH scatterplots were analyzed to investigate the spatial mismatch. All ischemic lesions in ADC, $APT^{\#}$, and rBTT images were automatically defined using a segmentation algorithm with K-means clustering technique (48). The hypoperfused area, showing a decrease in pH ($APT^{\#}$ deficit) without an ADC abnormality, was defined as pH/diffusion mismatch, corresponding to the ischemic acidosis penumbra, while the hypoperfused area with normal pH (isointense $APT^{\#}$ compared to the contralateral normal tissue) was defined as perfusion/pH mismatch, corresponding to the benign oligemia. Voxel values were normalized by the mean value of the contralateral normal tissue to generate relative values (rADC, $rAPT^{\#}$, and rBTT). In order to evaluate whether semi-solid MTC contributed to $APT^{\#}$ and NOE# images, MTR images ($= 1 - S_{sat}/S_0$) at 10 ppm were generated.

RESULTS

Figure 1a shows conventional, MTR_{asym}(3.5ppm), $APT^{\#}$, and NOE# MR images of an acute stroke patient (< 7 hrs from symptom onset) with right MCA occlusion. Both $APT^{\#}$ and NOE# images showed a strong hypointensity in the ischemic core identified from the DWI, while MTR_{asym}(3.5ppm) signal contrast between acidic ischemic lesion and contralateral normal brain tissue was relatively small. The Z-spectra, MTR_{asym} spectra, CEST# spectra, and NOE# spectra obtained from the ischemic stroke lesion and contralateral normal tissue are shown in Fig. 1b–e. Small MTR_{asym}(3.5ppm) contrast was observed between the ischemic lesion and contralateral normal tissue, although both MTR_{asym} spectra were negative at the higher frequency offset (> 4 ppm) due to large upfield NOE signal contributions. On the other hand, the NOE-free $APT^{\#}$ signal contrast was much larger than

the MTR_{asym}(3.5ppm) signal contrast. Interestingly, the upfield NOE# signal of the ischemic lesion was lower than that of the contralateral normal tissue.

Fig. 2 shows the serial multi-contrast MR images of a representative acute stroke patient with left MCA occlusion. DWI and ADC images showed local cytotoxic edema, generally leading to irreversible infarct. Perfusion-based rBTT and TTP maps showed perfusion deficits larger than diffusion deficits, and their spatial mismatch is typically used for the identification of salvageable penumbra. $APT^{\#}$ and NOE# images showed clear pH deficits in the ischemic lesion, whereas MTR_{asym}(3.5ppm) signals were only slightly hypointense. Interestingly, hyperintense $APT^{\#}$ signals were observed in a hemorrhage area (white arrows in Fig. 2) due to abundant mobile protein and peptide concentration in the blood, in line with previous investigations in rats (49). See Supporting Table S1 for quantitative analysis results and Supporting Fig. S1 for MTC-related maps.

Quantitatively, as shown in Fig. 3a, both $APT^{\#}$ and NOE# signals of the acidic ischemic lesion (1.41 ± 0.45 % for $APT^{\#}$ and 1.02 ± 0.40 % for NOE#) were significantly lower than those of the contralateral normal tissue (2.86 ± 0.36 % for $APT^{\#}$ and 2.08 ± 0.27 % for NOE#), while the MTR_{asym}(3.5ppm) signals showed a trend of reduction but no significant difference (0.78 ± 0.33 % for normal vs. 0.39 ± 0.46 % for lesion, $p = 0.071$). Correspondingly, the $APT^{\#}$ image contrast (NOE free) of the ischemic lesion (compared to the contralateral normal tissue) was also much larger than the MTR_{asym}(3.5ppm) image contrast (−1.45 ± 0.40 % for $APT^{\#}$ vs. −0.39 ± 0.52 % for MTR_{asym}(3.5ppm), $p = 4.6 \times 10–4$), as shown in Fig. 3b.

Fig. 4 shows pH/diffusion and perfusion/pH scatterplots to investigate the spatial dynamics of ischemia progression in a representative acute stroke patient with pH/perfusion mismatch, but minor diffusion/pH mismatch (Fig. 4a–c), and another patient with pH/perfusion mismatch, as well as diffusion/pH mismatch (Fig. 4d–f). Areas of reduced pH were larger than or equal to diffusion deficits, and smaller than perfusion deficits in the acute stroke phase. Of the thirteen patients scanned at acute phase (< 7 hrs), three patients showed pH/diffusion mismatch. The relative volume of the pH/diffusion mismatch to the infarct core and perfusion/pH mismatch were 0.21 and 0.34, respectively. The mean $rAPT^{\#}$ signals were 0.52, 0.62, and 0.97 for infarct core, pH/diffusion mismatch, and perfusion/pH mismatch.

Fig. 5 shows the averaged Z-spectra (a), MTR_{asym} spectra (b), and CEST# and NOE# spectra (c) obtained from the ischemic acidosis penumbra (pH/diffusion mismatch area, n=3). No significant difference was observed in mean MTR(10ppm) signal intensities between the normal (26.9 ± 4.1 %) and the ischemic acidosis penumbra (27.3 ± 3.1 %). The $APT^{\#}$ image contrast of the ischemic acidosis penumbra (compared to the contralateral normal tissue) was larger than the MTR_{asym}(3.5ppm) image contrast (−1.08 ± 0.43 % for $APT^{\#}$ vs. −0.51 ± 0.48 % for MTR_{asym}(3.5ppm), $p = 2.9 \times 10–3$).

DISCUSSION

In this study, we investigated the possibility of using the pH-weighted APT imaging to detect acidified ischemic stroke lesions and a pH-based acidosis penumbra in acute stroke

patients. APT studies interpreted using the EMR approach showed less contaminated APT-MRI signals, and concomitant enhanced APT-MRI sensitivity to pH, allowing reliable delineation of an ischemic acidosis penumbra. The spatial distributions of the diffusion deficits, pH-diffusion mismatches, and perfusion-pH mismatches suggest that hypoperfused acidic ischemic lesions without an ADC abnormality identified the ischemic acidosis penumbra, while the hypoperfused neural area classified benign oligemia in line with the hypotheses previously suggested (26, 27, 48). Interestingly, the intracerebral hemorrhage and ischemic stroke lesions showed opposite APT signal features which are hyperintensity and hypointensity compared with the contralateral normal brain tissue, respectively. Theoretically, two major sources of APT signals are the intracellular water-exchangeable amide proton content in the cytoplasm and its base-catalyzed exchange rate at physiological pH range (pH 6.5 ~ 7.5) (35, 45, 50). Consequently, hypointense APT signals in ischemic stroke were primarily attributable to local tissue acidosis while hyperintense APT signals in hemorrhage were attributable to the presence of rich mobile proteins and peptides in the blood (51). These observations confirm that APT imaging can separate hemorrhagic stroke from cerebral ischemic stroke, in line with previous observations (49).

The data indicate that the pH-dependent APT contribution to the MTR_{asym}(3.5ppm) signal intensity is reduced by the pH-dependent upfield relayed NOE signal contribution, and can even become negative particularly when a relatively low RF saturation power is applied (52). When using this APTw contrast to study tumors, it increases because the NOE is smaller in the tumor than in the normal tissue (36, 37). Thus, the NOE is actually a symbiotic factor for the MTR_{asym}(3.5ppm) image contrast in tumor studies. However, the NOE is a negative confounding factor in APT imaging of stroke. This is not surprising in view of the fact that, in mobile proteins, the relayed-NOE effect via exchangeable groups is pH dependent (35, 53–55). Therefore, the absolute MTR_{asym}(3.5ppm) signal intensity as well as the contrast of the ischemic stroke is reduced by the upfield NOE signals and the use of the asymmetry metric reduces the sensitivity of APT signals in ischemic stroke imaging. It should be mentioned that, contrary to our findings and the basic evidence from studies on cells and tissue (53) and high resolution NMR studies of proteins (56, 57), others have not found a change of relayed-NOE signals following acute stroke (29, 58, 59). The most likely explanation of this is a difference in saturation power B_1, leading to very different contributions of fast and slow exchanging protons to the Z-spectrum (60). At lower B_1 (about less than 1–2 μT), the CEST effect observed in a Z-spectrum is dominated by downfield slowly exchanging amide and upfield relayed-NOE protons, while at higher B_1 this is taken over by downfield fast exchanging protons (amine and hydroxyl), with large MTC on both sides. The MTC has shown little pH dependence due to the majority of contrast coming from direct dipolar transfer and molecular (H_2O) exchange, so at higher B_1, the pH dependency upfield will no longer be apparent. In the B_1 regime at 3T used for our studies, the amine contribution is expected to be minimal, but we expect some effect from the guanidinium protons in creatine around 2 ppm (exchange rate of about 950 Hz at physiological pH and a strong pH dependence between pH 6 and 7.5 (61)). The EMR fitting is very simple and removes most of the effects of MTC and direct saturation. It should not be affected by pH dependence much. Also, we use the symmetric MTC fitting. Thus, any fitting error would cause the NOE# and $APT^{\#}$ signals to be symmetric, which is not the case.

Accurate identification of the ischemic penumbra versus irreversible infarct tissue in the acute stroke clinical setting has great potential for guiding therapeutic decision-making, particularly for patients who present in an unknown or delayed time window. A spatial mismatch between diffusion and perfusion deficits has been used as a surrogate marker for salvageable tissue. However, this approach is known to overestimate the volume of penumbra in areas of benign oligemia. A static perfusion deficit does not capture the dynamic response to ischemia known to occur at the molecular level (18). Thus, when making decisions about costly and potentially harmful interventions for the treatment of acute stroke, perfusion imaging can be misleading, resulting in higher morbidity and mortality rates due to in appropriate interventions (17, 62–64). However, when impaired perfusion is significant enough to affect metabolism, a systemic intracellular acidosis ensues propagating out from a central infarct core, sparing regions of oligemia that have not resulted in anaerobic metabolism. Our observations show that pH deficits are smaller than perfusion deficits and equal to or larger than diffusion deficits, in line with previous animal studies (26, 27, 48). The pH deficit may reflect the area of final infarction expected without reperfusion and thus, the acidosis-based penumbra. The mismatch region between diffusion and pH deficits is expected to be a potential therapeutic target that is more specific than the PWI/DWI mismatch. Moreover, early and accurate identification of the acidosis-based penumbra with a size-based threshold may assist to select patients for delayed recanalization or neuroprotective treatment.

APT signals measured by a subtraction-based method (e.g., Z_{ref} - Z_{lab} where Z_{ref} and Z_{lab} are the normalized reference image signal intensity and the label image signal intensity with respect to S_0) depend on not only amide proton concentration and its exchange rate, but depending on the model used (e.g. Lorentzian fitting) also on semi-solid MTC effects and experimental conditions. Various types of pathology can alter tissue properties, particularly, water relaxation times, water content, and semi-solid MTC content. Previous studies showed that APT signal apparently increases with T_{1w}, but the relationship is not linear (42, 65). Notably, the positive correlation no longer exists at the high RF saturation power level, and it seems that the APT signal is not associated with T_{1w} at 2 μT, as was used in this study. In addition, our result showed that there was no significant MTR(10ppm) difference between normal brain tissue and stroke at 1 day time point (Supporting Table S1), which is in agreement with those of prior studies (66, 67). These authors found that the change of MTC was less than 1 % during initial few hours after stroke onset time. Furthermore, as shown in Fig. 2, MTR and $APT^{\#}$ images demonstrated very different contrast features, and the MTR contrasts were not projected onto the $APT^{\#}$ images, although obvious MTR contrasts were seen at 1 week. The results suggest that semisolid MTC contribution to the $APT^{\#}$ contrast between normal and ischemic areas was insignificant. Broad CEST signals were observed over a frequency range from 1 to 4 ppm, as shown in Fig. 1e and 5c. We attribute this to the pH effects of other exchangeable groups that are not exactly at 3.5 ppm, for instance, including the guanidinium protons of creatine and some amines (28, 68, 69). These CEST signals may also exist at the frequency offset of 0.5 ppm and may influence EMR fitting.

There are several limitations that need to be mentioned. First, T_{sat} on human scanners is often limited to < 1 sec due to hardware constraints (particularly the pulse length and the RF amplifier duty cycle) and specific absorption rate (SAR) requirements. In addition, a

moderate TR is typically employed to reduce the scan time for patients. When a short TR or relaxation delay length (= TR - T_{sat}), compared with T_1 relaxation time, is applied, the initial water longitudinal magnetization is reduced, resulting in a decrease in APT effect. However, it has been reported that APT signals obtained under strong RF saturation power can reach a maximum faster, while APT signals from weak RF saturation power slowly increased and reached a plateau at a longer RF saturation time (70, 71). Thus, the optimal saturation time under a relatively high RF saturation power is significantly shorter than what is designed to reach the steady-state under a low RF saturation power on animal scanners. Despite large semisolid MTC and direct water saturation effects, a relatively high RF saturation power (~ 2 μT) with a T_{sat} of 500~800 ms on 3 T human scanners has been used in previous stroke patient studies in an effort to achieve higher MTR_{asym}(3.5ppm) contrast within the specific absorption rate limit (30, 72). Of course, further studies may be needed to determine the optimal RF saturation power level for maximizing ischemic stroke contrast and increasing specificity to the APT effect. Second, the use of single-slice APT image acquisition for monitoring longitudinal changes in pH/diffusion mismatch is challenging. Instead, volumetric APT imaging is essential to evaluate whether pH/diffusion mismatch can predict the final infarct size if no recanalization occurs, or whether the final infarct size is reduced if recanalization occurs to salvage ischemic penumbra in hyperacute patients. Consequently, a very fast volumetric APT imaging technique that can be included in a comprehensive MR stroke protocol is required for hyperacute stroke patients (73–76). Third, in this study, we demonstrated substantially enhanced APT sensitivity to pH using the EMR analysis technique and better detection of a pH-based acidosis penumbra in acute stroke patients. However, definitive evidence is still lacking even though previous animal studies exhibited promising results (24–29). Thus, future research is needed to validate that the ischemic acidosis penumbra can predict final infarction size and outcome through prospective and/or retrospective cohort studies. Fourth, interestingly, we observed that the NOE# and MTR_{asym}(3.5ppm) signal contrasts were quite similar at 24 hrs acute stage (−0.9 % for NOE# and −0.96 % for MTR_{asym}(3.5ppm), see Supporting Fig. S2), whereas the contrast of the NOE# signal (−1.06 %) was higher than that of MTR_{asym}(3.5ppm) (−0.39 %) at all hyperacute, acute, and subacute stages (2 hrs to 5 days) as shown in Fig. 3, probably due to variable temporal evolution of APT and NOE signals. Further study, perhaps together with intracellular pH measurements using 31P MRS, is needed to reveal clear mechanisms.

CONCLUSIONS

APTw imaging based on MTR asymmetry analysis has shown promise for identifying ischemic lesions, but suffers from low accuracy due to small APTw intensity changes. In this study, quantitative $APT^{\#}$, NOE#, perfusion and diffusion MRI were performed on acute stroke patients. Our results showed that while APTw MRI for pH analysis based on MTR_{asym} analysis was confounded by upfield pH-sensitive NOE effects of mobile proteins and peptides, NOE-free APT-MRI contrast between normal and ischemic lesions was substantially increased, nearly 3 times larger than that based on MTR_{asym} analysis. Consequently, APT studies using the EMR approach can achieve less contaminated APT-MRI signals and enhance APT MRI sensitivity to pH, thus allowing more reliable delineation of an ischemic acidosis penumbra. This should be useful to help guide

thrombolytic and/or neuroprotective therapies for acute stroke patients at various therapeutic windows.

Supplementary Material

Refer to Web version on PubMed Central for supplementary material.

Acknowledgments

This research was possible because of contributions from the NIH Natural History of Stroke Investigators who are: Richard T. Benson, Amie W. Hsia, Lawrence L. Latour, Richard Leigh, Marie Luby, John K. Lynch, Jose G. Merino, Zurab Nadareishvili, and Steven J. Warach. We thank Dr. Linda Knutsson for insight regarding the DSC perfusion parameters. This work was supported in part by grants from the National Institutes of Health (R01NS083435, R01CA166171, R01EB009731, R01EB015032, and P41EB015909) and by the National Institute of Neurological Disorders and Stroke (NINDS) Intramural Research Program of the NIH.

References

1. Astrup J, Siesjo BK, Symon L. Thresholds in cerebral ischemia - the ischemia penumbra. Stroke. 1981; 12:723–725. [PubMed: 6272455]
2. Warach S, Dashe JF, Edelman RR. Clinical outcome in ischemic stroke predicted by early diffusion-weighted and perfusion magnetic resonance imaging: a preliminary analysis. J Cereb Blood Flow Metab. 1996; 16:53–59. [PubMed: 8530555]
3. Barber PA, Darby DG, Desmond PM, Yang Q, Gerraty RP, Jolley D, Donnan GA, Tress BM, Davis SM. Prediction of stroke outcome with echoplanar perfusion- and diffusion-weighted MRI. Neurology. 1998; 51:418–426. [PubMed: 9710013]
4. Schwamm LH, Koroshetz WJ, Sorensen AG, Wang B, Copen WA, Budzik R, Rordorf G, Buonanno FS, Schaefer PW, Gonzalez RG. Time course of lesion development in patients with acute stroke: serial diffusion- and hemodynamic-weighted magnetic resonance imaging. Stroke. 1998; 29:2268–2276. [PubMed: 9804633]
5. Neumann-Haefelin T, Wittsack HJ, Wenserski F, Siebler M, Seitz RJ, Modder U, Freund HJ. Diffusion-and perfusion-weighted MRI - The DWI/PWI mismatch region in acute stroke. Stroke. 1999; 30:1591–1597. [PubMed: 10436106]
6. Hacke W, Kaste M, Bluhmki E, Brozman M, Davalos A, Guidetti D, Larrue V, Lees KR, Medeghri Z, Machnig T, Schneider D, von Kummer R, Wahlgren N, Toni D. Thrombolysis with alteplase 3 to 4.5 hours after acute ischemic stroke. N Engl J Med. 2008; 359:1317–1329. [PubMed: 18815396]
7. Wechsler LR. Intravenous thrombolytic therapy for acute ischemic stroke. N Engl J Med. 2011; 364:2138–2146. [PubMed: 21631326]
8. Saver JL, Fonarow GC, Smith EE, Reeves MJ, Grau-Sepulveda MV, Pan W, Olson DM, Hernandez AF, Peterson ED, Schwamm LH. Time to treatment with intravenous tissue plasminogen activator and outcome from acute ischemic stroke. JAMA. 2013; 309:2480–2488. [PubMed: 23780461]
9. Lansberg MG, Straka M, Kemp S, Mlynash M, Wechsler LR, Jovin TG, Wilder MJ, Lutsep HL, Czartoski TJ, Bernstein RA, Chang CW, Warach S, Fazekas F, Inoue M, Tipirneni A, Hamilton SA, Zaharchuk G, Marks MP, Bammer R, Albers GW. MRI profile and response to endovascular reperfusion after stroke (DEFUSE 2): a prospective cohort study. Lancet Neurol. 2012; 11:860–867. [PubMed: 22954705]
10. Leigh R, Jen SS, Hillis AE, Krakauer JW, Barker PB. Pretreatment blood-brain barrier damage and post-treatment intracranial hemorrhage in patients receiving intravenous tissue-type plasminogen activator. Stroke. 2014; 45:2030–2035. [PubMed: 24876245]
11. Albers GW, Thijs VN, Wechsle L, Kemp S, Schlaug G, Skalabrin E, Bammer R, Kakuda W, Lansberg MG, Shuaib A, Coplin W, Scott H, Moseley M, Marks MP. Magnetic resonance imaging profiles predict clinical response to early reperfusion: The diffusion and perfusion imaging evaluation for understanding stroke evolution (DEFUSE) study. Ann Neurology. 2006; 60:508–517.

12. Schlaug G, Benfield A, Baird AE, Siewert B, Lovblad KO, Parker RA, Edelman RR, Warach S. The ischemic penumbra - Operationally defined by diffusion and perfusion MRI. Neurology. 1999; 53:1528–1537. [PubMed: 10534263]
13. Davis SM, Donnan GA, Parsons MW, Levi C, Butcher KS, Peeters A, Barber PA, Bladin C, De Silva DA, Byrnes G, Chalk JB, Fink JN, Kimber TE, Schultz D, Hand PJ, Frayne J, Hankey G, Muir K, Gerraty R, Tress BM, Desmond PM. Effects of alteplase beyond 3 h after stroke in the Echoplanar Imaging Thrombolytic Evaluation Trial (EPITHET): a placebo-controlled randomised trial. Lancet Neurology. 2008; 7:299–309. [PubMed: 18296121]
14. Gonzalez RG, Schaefer PW, Buonanno FS, Schwamm LH, Budzik RF, Rordorf G, Wang B, Sorensen AG, Koroshetz WJ. Diffusion-weighted MR imaging: Diagnostic accuracy in patients imaged within 6 hours of stroke symptom onset. Radiology. 1999; 210:155–162. [PubMed: 9885601]
15. Chalela JA, Kidwell CS, Nentwich LM, Luby M, Butman JA, Demchuk AM, Hill MD, Patronas N, Latour L, Warach S. Magnetic resonance imaging and computed tomography in emergency assessment of patients with suspected acute stroke: a prospective comparison. Lancet. 2007; 369:293–298. [PubMed: 17258669]
16. Morita S, Suzuki M, Iizuka K. False-negative diffusion-weighted MRI in acute cerebellar stroke. Auris Nasus Larynx. 2011; 38:577–582. [PubMed: 21330074]
17. Kucinski T, Naumann D, Knab R, Schoder V, Wegener S, Fiehler J, Majumder A, Rother J, Zeumer H. Tissue at risk is overestimated in perfusion weighted imaging: MR imaging in acute stroke patients without vessel recanalization. AJNR Am J Neuroradiol. 2005; 26:815–819. [PubMed: 15814926]
18. Hossmann KA. Pathophysiological basis of translational stroke research. Folia Neuropathol. 2009; 47:213–227. [PubMed: 19813140]
19. Guadagno JV, Donnan GA, Markus R, Gillard JH, Baron JC. Imaging the ischaemic penumbra. Curr Opin Neurol. 2004; 17:61–67. [PubMed: 15090879]
20. Heiss WD. Ischemic penumbra: evidence from functional imaging in man. J Cereb Blood Flow Metab. 2000; 20:1276–1293. [PubMed: 10994849]
21. Leigh R, Knutsson L, Zhou J, van Zijl PC. Imaging the physiological evolution of the ischemic penumbra in acute ischemic stroke. J Cereb Blood Flow Metab. 2017; doi: 10.1177/0271678X17700913
22. Hossmann KA. Viability thresholds and the penumbra of focal ischemia. Ann Neurol. 1994; 36:557–565. [PubMed: 7944288]
23. Siesjo BK. Pathophysiology and treatment of focal cerebral ischemia. J Neurosurg. 1992; 77:337–354. [PubMed: 1506880]
24. Zhou J, Payen J, Wilson DA, Traystman RJ, van Zijl PCM. Using the amide proton signals of intracellular proteins and peptides to detect pH effects in MRI. Nature Med. 2003; 9:1085–1090. [PubMed: 12872167]
25. Sun PZ, Zhou J, Huang J, van Zijl P. Simplified quantitative description of amide proton transfer (APT) imaging during acute ischemia. Magn Reson Med. 2007; 57:405–410. [PubMed: 17260362]
26. Sun PZ, Zhou J, Sun W, Huang J, van Zijl PCM. Detection of the ischemic penumbra using pH-weighted MRI. J Cereb Blood Flow Metab. 2007; 27:1129–1136. [PubMed: 17133226]
27. Zhou J, van Zijl PC. Defining an Acidosis-Based Ischemic Penumbra from pH-Weighted MRI. Transl Stroke Res. 2011; 3:76–83. [PubMed: 22408691]
28. Jin T, Wang P, Zong XP, Kim SG. Magnetic resonance imaging of the Amine-Proton EXchange (APEX) dependent contrast. NeuroImage. 2012; 59:1218–1227. [PubMed: 21871570]
29. Jin T, Wang P, Zong X, Kim SG. MR imaging of the amide-proton transfer effect and the pH-insensitive nuclear overhauser effect at 9.4 T. Magn Reson Med. 2013; 69:760–770. [PubMed: 22577042]
30. Zhao X, Wen Z, Huang F, Lu S, Wang X, Hu S, Zu D, Zhou J. Saturation power dependence of amide proton transfer image contrasts in human brain tumors and strokes at 3 T. Magn Reson Med. 2011; 66:1033–1041. [PubMed: 21394783]
31. Tee YK, Harston GW, Blockley N, Okell TW, Levman J, Sheerin F, Cellerini M, Jezzard P, Kennedy J, Payne SJ, Chappell MA. Comparing different analysis methods for quantifying the

MRI amide proton transfer (APT) effect in hyperacute stroke patients. NMR Biomed. 2014; 27:1019–1029. [PubMed: 24913989]

32. Tietze A, Blicher J, Mikkelsen IK, Ostergaard L, Strother MK, Smith SA, Donahue MJ. Assessment of ischemic penumbra in patients with hyperacute stroke using amide proton transfer (APT) chemical exchange saturation transfer (CEST) MRI. NMR Biomed. 2014; 27:163–174. [PubMed: 24288260]
33. Harston GW, Tee YK, Blockley N, Okell TW, Thandeswaran S, Shaya G, Sheerin F, Cellerini M, Payne S, Jezzard P, Chappell M, Kennedy J. Identifying the ischaemic penumbra using pH-weighted magnetic resonance imaging. Brain. 2015; 138:36–42. [PubMed: 25564491]
34. Ling W, Regatte RR, Navon G, Jerschow A. Assessment of glycosaminoglycan concentration in vivo by chemical exchange-dependent saturation transfer (gagCEST). Proc Natl Acad Sci (USA). 2008; 105:2266–2270. [PubMed: 18268341]
35. van Zijl PCM, Yadav NN. Chemical exchange saturation transfer (CEST): What is in a name and what isn't? Magn Reson Med. 2011; 65:927–948. [PubMed: 21337419]
36. Heo HY, Zhang Y, Jiang S, Lee DH, Zhou J. Quantitative assessment of amide proton transfer (APT) and nuclear overhauser enhancement (NOE) imaging with extrapolated semisolid magnetization transfer reference (EMR) signals: II. Comparison of three EMR models and application to human brain glioma at 3 Tesla. Magn Reson Med. 2016; 75:1630–1639. [PubMed: 26033553]
37. Heo HY, Zhang Y, Lee DH, Hong X, Zhou J. Quantitative assessment of amide proton transfer (APT) and nuclear overhauser enhancement (NOE) imaging with extrapolated semi-solid magnetization transfer reference (EMR) signals: Application to a rat glioma model at 4.7 tesla. Magn Reson Med. 2016; 75:137–149. [PubMed: 25753614]
38. Henkelman RM, Huang X, Xiang QS, Stanisz GJ, Swanson SD, Bronskill MJ. Quantitative interpretation of magnetization transfer. Magn Reson Med. 1993; 29:759–766. [PubMed: 8350718]
39. Sled JG, Pike GB. Quantitative imaging of magnetization transfer exchange and relaxation properties in vivo using MRI. Magn Reson Med. 2001; 46:923–931. [PubMed: 11675644]
40. Kim M, Gillen J, Landman BA, Zhou J, van Zijl PC. Water saturation shift referencing (WASSR) for chemical exchange saturation transfer (CEST) experiments. Magn Reson Med. 2009; 61:1441–1450. [PubMed: 19358232]
41. Zhang Y, Heo HY, Lee DH, Zhao X, Jiang S, Zhang K, Li H, Zhou J. Selecting the reference image for registration of CEST series. J Magn Reson Imaging. 2016; 43:756–761. [PubMed: 26268435]
42. Heo HY, Lee DH, Zhang Y, Zhao X, Jiang S, Chen M, Zhou J. Insight into the quantitative metrics of chemical exchange saturation transfer (CEST) imaging. Magn Reson Med. 2016; doi: 10.1002/mrm.26264
43. Lee DH, Heo HY, Zhang K, Zhang Y, Jiang S, Zhao X, Zhou J. Quantitative assessment of the effects of water proton concentration and water T changes on amide proton transfer (APT) and nuclear overhauser enhancement (NOE) MRI: The origin of the APT imaging signal in brain tumor. Magn Reson Med. 2016; doi: 10.1002/mrm.26131
44. Heo HY, Jones CK, Hua J, Yadav N, Agarwal S, Zhou J, van Zijl PC, Pillai JJ. Whole-brain amide proton transfer (APT) and nuclear overhauser enhancement (NOE) imaging in glioma patients using low-power steady-state pulsed chemical exchange saturation transfer (CEST) imaging at 7T. J Magn Reson Imaging. 2016; 44:41–50. [PubMed: 26663561]
45. Zhou J, Wilson DA, Sun PZ, Klaus JA, Van Zijl PC. Quantitative description of proton exchange processes between water and endogenous and exogenous agents for WEX, CEST, and APT experiments. Magn Reson Med. 2004; 51:945–952. [PubMed: 15122676]
46. Quesson B, Thiaudiere E, Delalande C, Chateil JF, Moonen CT, Canioni P. Magnetization transfer imaging of rat brain under non-steady-state conditions. Contrast prediction using a binary spin-bath model and a super-lorentzian lineshape. J Magn Reson. 1998; 130:321–328. [PubMed: 9500906]
47. Ethofer T, Mader I, Seeger U, Helms G, Erb M, Grodd W, Ludolph A, Klose U. Comparison of longitudinal metabolite relaxation times in different regions of the human brain at 1.5 and 3. Tesla Magn Reson Med. 2003; 50:1296–1301. [PubMed: 14648578]

48. Guo Y, Zhou IY, Chan ST, Wang Y, Mandeville ET, Igarashi T, Lo EH, Ji X, Sun PZ. pH-sensitive MRI demarcates graded tissue acidification during acute stroke - pH specificity enhancement with magnetization transfer and relaxation-normalized amide proton transfer (APT) MRI. Neuroimage. 2016; 141:242–249. [PubMed: 27444569]
49. Wang M, Hong X, Chang CF, Li Q, Ma B, Zhang H, Xiang S, Heo HY, Zhang Y, Lee DH, Jiang S, Leigh R, Koehler RC, van Zijl PC, Wang J, Zhou J. Simultaneous detection and separation of hyperacute intracerebral hemorrhage and cerebral ischemia using amide proton transfer MRI. Magn Reson Med. 2015; 74:42–50.
50. Zhou J, van Zijl PC. Chemical exchange saturation transfer imaging and spectroscopy. Progr NMR Spectr. 2006; 48:109–136.
51. Zheng S, van der Bom IM, Zu Z, Lin G, Zhao Y, Gounis MJ. Chemical exchange saturation transfer effect in blood. Magn Reson Med. 2014; 71:1082–1092. [PubMed: 23661508]
52. Zhou J, Hong X, Zhao X, Gao JH, Yuan J. APT-weighted and NOE-weighted image contrasts in glioma with different RF saturation powers based on magnetization transfer ratio asymmetry analyses. Magn Reson Med. 2013; 70:320–327. [PubMed: 23661598]
53. van Zijl PC, Zhou J, Mori N, Payen JF, Wilson D, Mori S. Mechanism of magnetization transfer during on-resonance water saturation. A new approach to detect mobile proteins, peptides, and lipids. Magn Reson Med. 2003; 49:440–449. [PubMed: 12594746]
54. Jones CK, Huang A, Xu J, Edden RA, Schar M, Hua J, Oskolkov N, Zaca D, Zhou J, McMahon MT, Pillai JJ, van Zijl PC. Nuclear Overhauser enhancement (NOE) imaging in the human brain at 7T. Neuroimage. 2013; 77:114–124. [PubMed: 23567889]
55. Xu J, Yadav NN, Bar-Shir A, Jones CK, Chan KW, Zhang J, Walczak P, McMahon MT, van Zijl PC. Variable delay multi-pulse train for fast chemical exchange saturation transfer and relayed-nuclear overhauser enhancement MRI. Magn Reson Med. 2014; 71:1798–1812. [PubMed: 23813483]
56. Otting G, Liepinsh E, Wuthrich K. Protein hydration in aqueous solution. Science. 1991; 254:974–980. [PubMed: 1948083]
57. Hwang TL, van Zijl PC, Mori S. Accurate quantitation of water-amide proton exchange rates using the phase-modulated CLEAN chemical EXchange (CLEANEX-PM) approach with a Fast-HSQC (FHSQC) detection scheme. J Biomol NMR. 1998; 11:221–226. [PubMed: 9679296]
58. Zhang XY, Wang F, Afzal A, Xu J, Gore JC, Gochberg DF, Zu Z. A new NOE-mediated MT signal at around -1.6ppm for detecting ischemic stroke in rat brain. Magn Reson Imaging. 2016; 34:1100–1106. [PubMed: 27211260]
59. Zaiss M, Windschuh J, Goerke S, Paech D, Meissner JE, Burth S, Kickingereder P, Wick W, Bendszus M, Schlemmer HP, Ladd ME, Bachert P, Radbruch A. Downfield-NOE-suppressed amide-CEST-MRI at 7 Tesla provides a unique contrast in human glioblastoma. Magn Reson Med. 2017; 77:196–208. [PubMed: 26845067]
60. van Zijl PCM, Lam WW, Xu J, Knutsson L, Stanisz GJ. Magnetization Transfer Contrast and Chemical Exchange Saturation Transfer MRI. Features and analysis of the field-dependent saturation spectrum. Neuroimage. 2017; doi: 10.1016/j.neuroimage.2017.1004.1045
61. Haris M, Nanga RP, Singh A, Cai K, Kogan F, Hariharan H, Reddy R. Exchange rates of creatine kinase metabolites: feasibility of imaging creatine by chemical exchange saturation transfer MRI. NMR Biomed. 2012; 25:1305–1309. [PubMed: 22431193]
62. Kidwell CS, Alger JR, Saver JL. Evolving paradigms in imaging the ischemic penumbra with multimodal magnetic resonance imaging. Stroke. 2003; 34:2729–2735. [PubMed: 14576370]
63. Bandera E, Botteri M, Minelli C, Sutton A, Abrams KR, Latronico N. Cerebral blood flow threshold of ischemic penumbra and infarct core in acute ischemic stroke - A systematic review. Stroke. 2006; 37:1334–1339. [PubMed: 16574919]
64. Ford AL, An HY, Vo KD, Lin WL, Lee JM. Defining the ischemic penumbra using hyperacute neuroimaging: Deriving quantitative ischemic thresholds. Transl Stroke Res. 2012; 3:198–204. [PubMed: 24323775]
65. Zhang XY, Wang F, Li H, Xu J, Gochberg DF, Gore JC, Zu Z. CEST imaging of fast exchanging amine pools with corrections for competing effects at 9.4 T. NMR Biomed. 2017; doi: 10.1002/nbm.3715

66. Makela HI, Kettunen MI, Grohn OH, Kauppinen RA. Quantitative T_{1r} and magnetic transfer magnetic resonance imaging of acute cerebral ischemia in the rat. J Cereb Blood Flow Metab. 2002; 22:547–558. [PubMed: 11973427]

67. Jokivarsi KT, Hiltunen Y, Grohn H, Tuunanen P, Grohn OH, Kauppinen RA. Estimation of the onset time of cerebral ischemia using T1rho and T2 MRI in rats. Stroke. 2010; 41:2335–2340. [PubMed: 20814006]

68. Cai K, Singh A, Poptani H, Li W, Yang S, Lu Y, Hariharan H, Zhou XJ, Reddy R. CEST signal at 2ppm (CEST@2ppm) from Z-spectral fitting correlates with creatine distribution in brain tumor. NMR Biomed. 2015; 28:1–8. [PubMed: 25295758]

69. Haris M, Singh A, Cai K, Kogan F, McGarvey J, Debrosse C, Zsido GA, Witschey WR, Koomalsingh K, Pilla JJ, Chirinos JA, Ferrari VA, Gorman JH, Hariharan H, Gorman RC, Reddy R. A technique for in vivo mapping of myocardial creatine kinase metabolism. Nat Med. 2014; 20:209–214. [PubMed: 24412924]

70. Xiao G, Sun PZ, Wu R. Fast simulation and optimization of pulse-train chemical exchange saturation transfer (CEST) imaging. Phys Med Biol. 2015; 60:4719–4730. [PubMed: 26020414]

71. Jin T, Autio J, Obata T, Kim SG. Spin-locking versus chemical exchange saturation transfer MRI for investigating chemical exchange process between water and labile metabolite protons. Magn Reson Med. 2011; 65:1448–1460. [PubMed: 21500270]

72. Zhou J, Blakeley JO, Hua J, Kim M, Laterra J, Pomper MG, van Zijl PC. Practical data acquisition method for human brain tumor amide proton transfer (APT) imaging. Magn Reson Med. 2008; 60:842–849. [PubMed: 18816868]

73. Zhu H, Jones CK, van Zijl PCM, Barker PB, Zhou J. Fast 3D chemical exchange saturation transfer (CEST) imaging of the human brain. Magn Reson Med. 2010; 64:638–644. [PubMed: 20632402]

74. Zhou J, Zhu H, Lim M, Blair L, Quinones-Hinojosa A, Messina AA, Eberhart CG, Pomper MG, Laterra J, Barker PB, van Zijl PCM, Blakeley JO. Three-dimensional amide proton transfer MR imaging of gliomas: Initial experience and comparison with gadolinium enhancement. J Magn Reson Imaging. 2013; 38:1119–1128. [PubMed: 23440878]

75. Zhang Y, Heo HY, Lee DH, Jiang S, Zhao X, Bottomley PA, Zhou J. Chemical exchange saturation transfer (CEST) imaging with fast variably-accelerated sensitivity encoding (vSENSE). Magn Reson Med. 2016

76. Heo HY, Zhang Y, Lee DH, Jiang S, Zhao X, Zhou J. Accelerating chemical exchange saturation transfer (CEST) MRI by combining compressed sensing and sensitivity encoding techniques. Magn Reson Med. 2017; 77:779–786. [PubMed: 26888295]

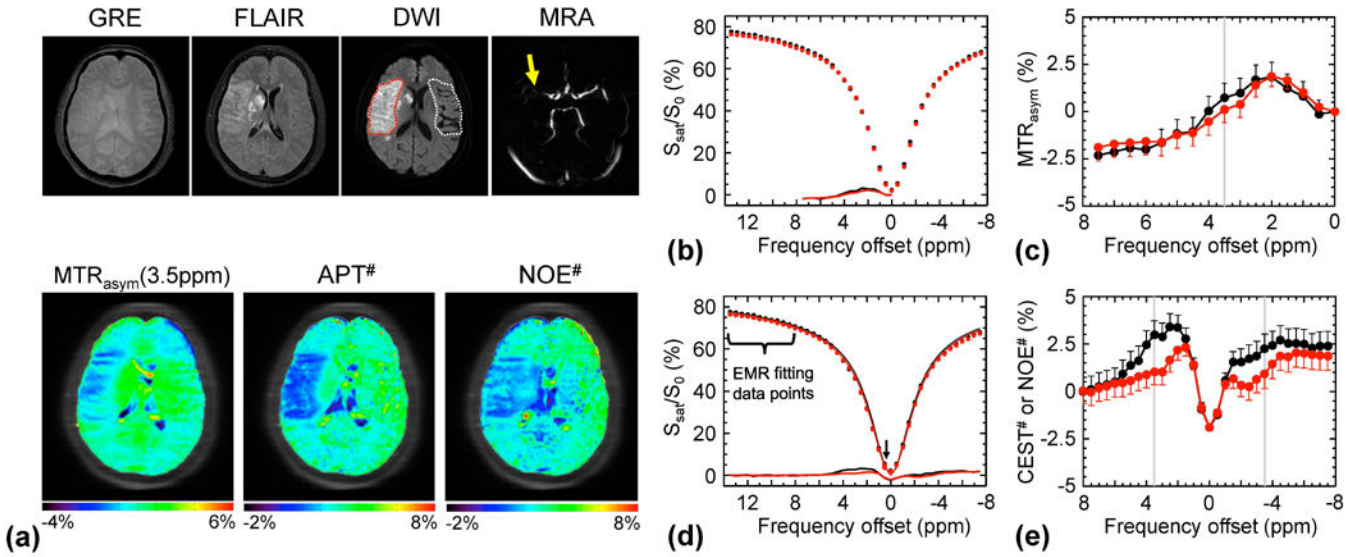

Figure 1.

APT-MRI quantification comparison of an acute stroke patient with right MCA occlusion (< 7 hrs from symptom onset) using the MTR asymmetry analysis and EMR approaches. **a:** MR images. Both APT$^{\#}$ and NOE# showed much clearer ischemic contrasts than MTR_{asym}(3.5ppm). **b, c:** Z-spectra and MTR_{asym} spectra obtained from the contralateral normal (black) and the ischemic lesion (red). **d:** Wide-offset Z-spectra with only MTC between 8 and 14 ppm, and extra 0.5 ppm (for improving fitting quality), were fitted to the two-pool MTC model. **e:** The quantitative CEST# signals obtained by subtracting the experimentally measured Z-spectra (red and black circles in d) from the EMR curve (red and black solid lines in d).

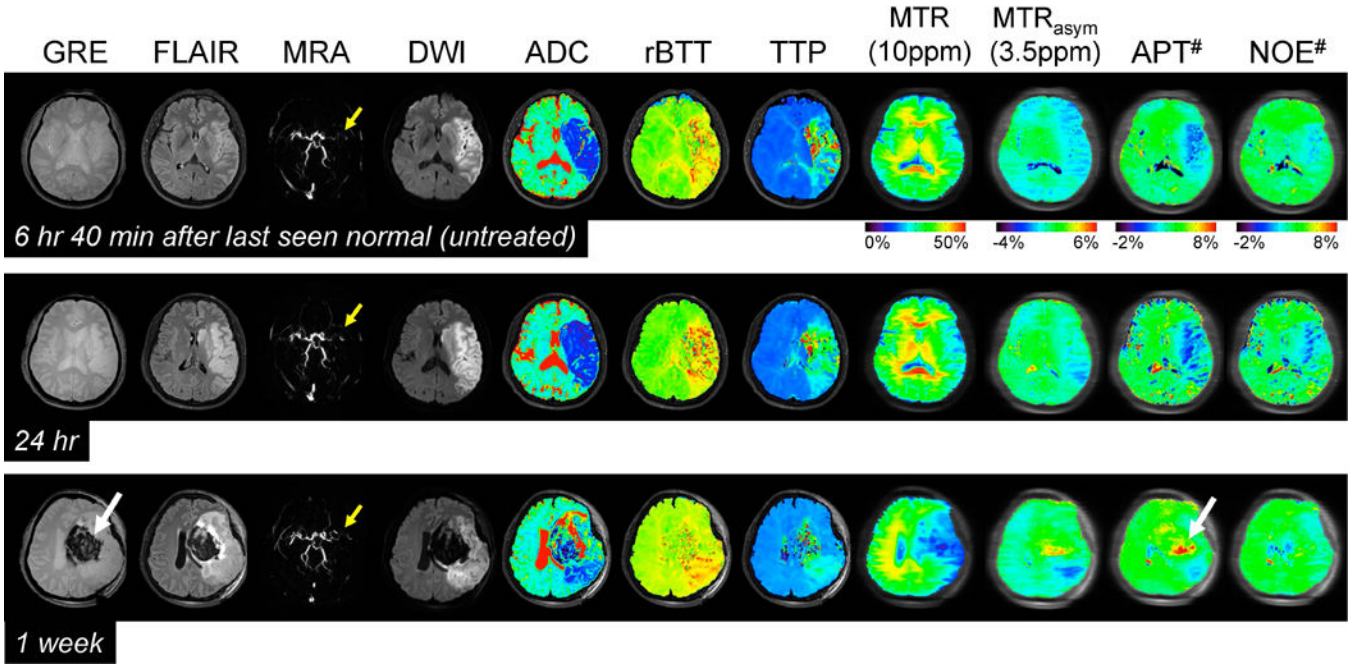

Figure 2.

Serial multimodality MR images of a representative acute stroke patient with left MCA occlusion (yellow arrows) at three time points. DWI and ADC showed large acute ischemic areas due to cytotoxic edema. In addition, perfusion-based rBTT and TTP showed obvious hypoperfusion in a slightly larger region than the diffusion abnormality. Both $APT^{\#}$ and NOE# showed much clearer ischemic contrasts than MTR_{asym}(3.5ppm) at two earlier time points. High APT signal intensities observed at 1 week can be attributed to a hemorrhage (white arrows) caused by abundant mobile proteins and peptides in the blood. Note that there was no significant contrast between normal and ischemic areas in MTR at 10 ppm within 1 day.

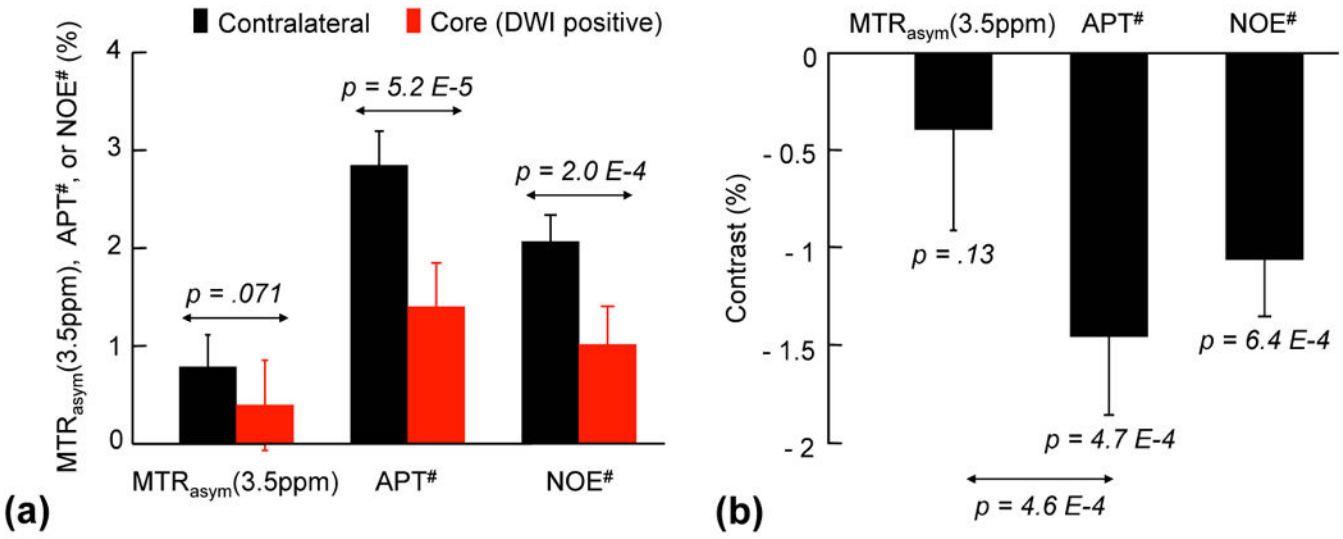

Figure 3.

Average MTR_{asym}(3.5ppm), $APT^{\#}$, and NOE# image intensities and contrasts between acidic ischemic and contralateral normal tissues from thirty acute stroke patients. **a:** Both $APT^{\#}$ and NOE# signal intensities of the ischemic lesion (DWI hyperintensity) were significantly lower than those of the contralateral normal tissue, while the MTR_{asym}(3.5ppm) signals showed no significant difference. **b:** The NOE free-$APT^{\#}$ image contrast between acidic ischemic and contralateral normal tissues outside the DWI lesion was much larger than the MTR_{asym}(3.5ppm) image contrast.

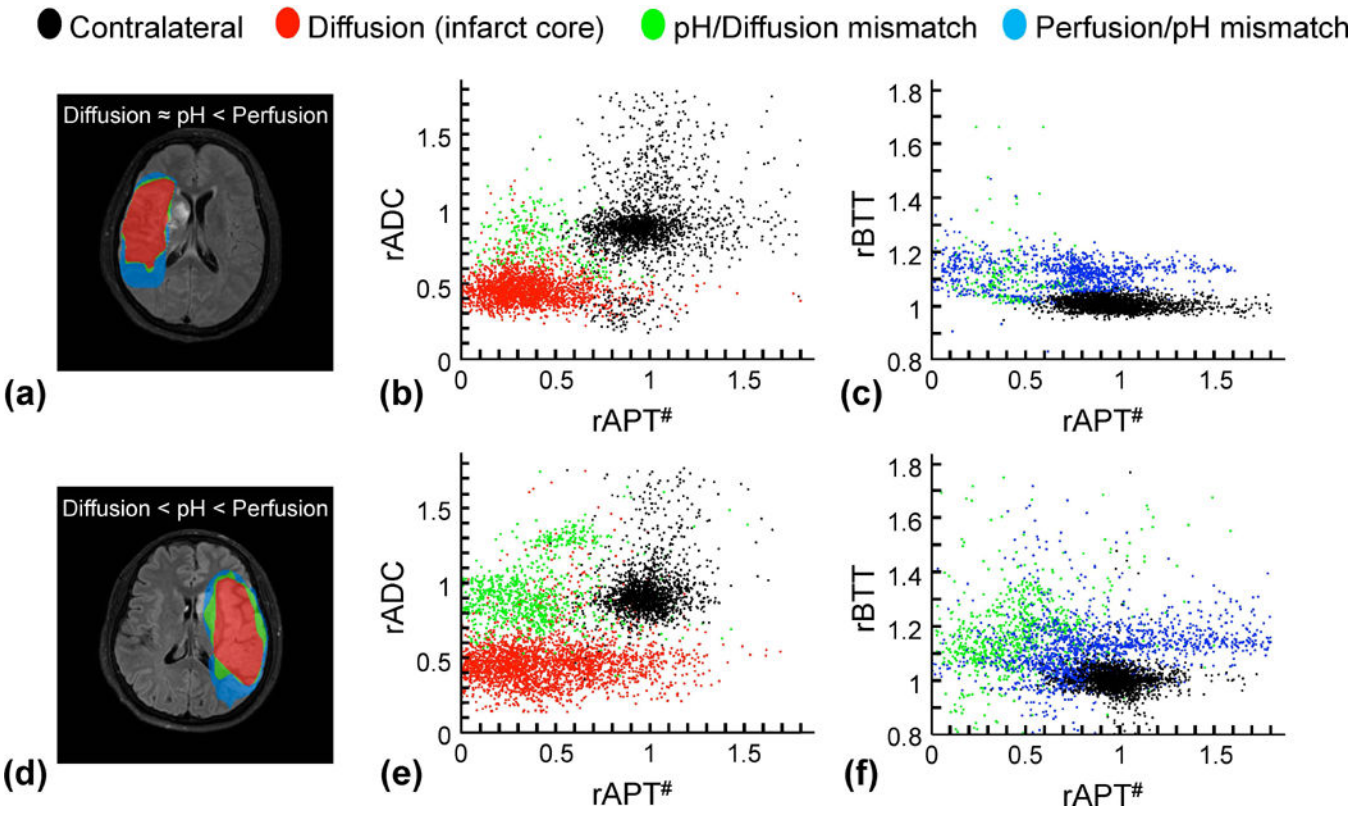

Figure 4.

Comparisons of diffusion/pH/perfusion deficits and quantitative pH/diffusion and perfusion/pH scatterplots in two acute stroke patients at 1 day from symptom onset. **a-c:** A patient with pH/perfusion mismatch, but minor diffusion/pH mismatch. **d–f:** A patient with pH/perfusion mismatch, as well as diffusion/pH mismatch. All ischemic lesions in ADC, APT$^{\#}$, and rBTT images were automatically segmented using an algorithm with k-means clustering technique. The distributions of the diffusion deficit area (infarct core, red), pH-diffusion mismatch (acidosis-based penumbra, green), and perfusion-pH mismatch (acidosis-based benign oligemia, blue) were markedly different from those of the contralateral normal tissue (black).

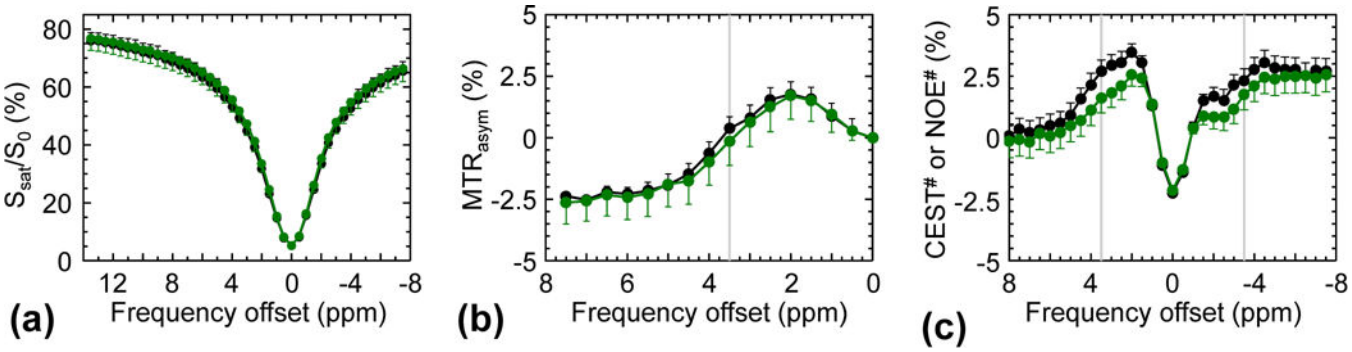

Figure 5.

Average Z-spectra (a), MTR_{asym} spectra (b), and $APT^{\#}$ and NOE# signals (c) obtained from the contralateral normal (black) and the diffusion/pH mismatch (green) from three acute stroke patients (< 7 hours from symptom onset).